ARTICLE OPEN

Protective effect of PDE4B subtype-specific inhibition in an *App* knock-in mouse model for Alzheimer's disease

Paul Armstrong[1,5], Hüseyin Güngör[2,3,5], Pariya Anongjanya[1], Clare Tweedy[1], Edward Parkin[2], Jamie Johnston[1], Ian M. Carr[4], Neil Dawson[2] and Steven J. Clapcote[1 ✉]

Meta-analysis of genome-wide association study data has implicated *PDE4B* in the pathogenesis of Alzheimer's disease (AD), the leading cause of senile dementia. *PDE4B* encodes one of four subtypes of cyclic adenosine monophosphate (cAMP)-specific phosphodiesterase-4 (PDE4A–D). To interrogate the involvement of PDE4B in the manifestation of AD-related phenotypes, the effects of a hypomorphic mutation (*Pde4b*[Y358C]) that decreases PDE4B's cAMP hydrolytic activity were evaluated in the *App*[NL-G-F] knock-in mouse model of AD using the Barnes maze test of spatial memory, ^{14}C-2-deoxyglucose autoradiography, thioflavin-S staining of β-amyloid (Aβ) plaques, and inflammatory marker assay and transcriptomic analysis (RNA sequencing) of cerebral cortical tissue. At 12 months of age, *App*[NL-G-F] mice exhibited spatial memory and brain metabolism deficits, which were prevented by the hypomorphic PDE4B in *App*[NL-G-F]/*Pde4b*[Y358C] mice, without a decrease in Aβ plaque burden. RNA sequencing revealed that, among the 531 transcripts differentially expressed in *App*[NL-G-F] versus wild-type mice, only 13 transcripts from four genes – *Ide*, *Btaf1*, *Padi2,* and *C1qb* – were differentially expressed in *App*[NL-G-F]/*Pde4b*[Y358C] versus *App*[NL-G-F] mice, identifying their potential involvement in the protective effect of hypomorphic PDE4B. Our data demonstrate that spatial memory and cerebral glucose metabolism deficits exhibited by 12-month-old *App*[NL-G-F] mice are prevented by targeted inhibition of PDE4B. To our knowledge, this is the first demonstration of a protective effect of PDE4B subtype-specific inhibition in a preclinical model of AD. It thus identifies PDE4B as a key regulator of disease manifestation in the *App*[NL-G-F] model and a promising therapeutic target for AD.

Neuropsychopharmacology; https://doi.org/10.1038/s41386-024-01852-z

INTRODUCTION

Alzheimer's disease (AD) is the leading cause of dementia and disability in old age, with pathological features including extracellular plaque deposits of the β-amyloid (Aβ) peptide and an estimated heritability of ~60% [1–3]. Although recent clinical trials of Aβ-targeting monoclonal antibodies resulted in moderately less cognitive decline in people with early AD [4, 5], no therapeutics capable of halting or reversing the progression of the disease have been described.

The risk of developing senile dementia is 34% higher in individuals with gastroesophageal reflux disease (GERD) compared with controls [6]. Meta-analysis of genome-wide association study (GWAS) data indicates that AD and GERD share seven genome-wide significant susceptibility loci [7]. Among the implicated genes, *PDE4B*, encoding one of four subtypes of cyclic adenosine monophosphate (cAMP)-specific phosphodiesterase-4 (PDE4A–D), was proposed as a plausible therapeutic target that should be investigated further [7].

Across various tissues, PDE4B is expressed in five isoforms (PDE4B1–5) [8]. In adult mammalian brain tissue, *Pde4b* transcripts have been identified by single-cell RNA sequencing in nearly all subclasses of GABAergic (gamma-aminobutyric acidergic) inhibitory neurons and glutamatergic excitatory neurons, and in some types of glial cell (Figs. S1 and S2) [9, 10]. PDE4B transcription was shown to be upregulated in primary rat microglial cell cultures by exposure to Aβ peptides, resulting in induction of the inflammatory cytokine TNFα, which was markedly decreased by the non-subtype-selective (pan-) PDE4 inhibitor rolipram (targeting all of four subtypes, PDE4A–D) [11].

The super-family of phosphodiesterases (PDE1–11) has long been considered as potential targets for AD therapy [12–19]. Transgenic amyloid precursor protein (APP)-overexpressing mouse models of AD have shown amelioration of cognitive deficits following treatment with the pan-PDE4 inhibitors rolipram [20–22], roflumilast [23, 24] and FFPM [25], and with the PDE4D subtype-selective inhibitors GEBR-7b [26] and GEBR-32a [27]. Rolipram had no effect on Aβ peptide levels or plaque load in the PS/APP and Tg2576 strains [20, 21], although treatment over 24 days was shown to decrease Aβ peptide levels in brain tissue from 11-month-old 3xTg-AD mice [22]. Prior to the genetic validation of PDE4B by the GWAS meta-analysis [7], no work had been published in this context specifically on the PDE4B subtype.

We previously showed that a hypomorphic mutation (*Pde4b*[Y358C]), which affects all PDE4B isoforms and decreases the enzyme's cAMP hydrolytic activity by 27%, results in increased phosphorylation of CREB (cAMP response element binding protein) and cognitive

enhancement in young adult (12-week-old) C57BL/6J mice [28]. To interrogate the involvement of PDE4B in the manifestation of AD-related phenotypes, we evaluated the neurocognitive effects of the $Pde4b^{Y358C}$ hypomorph in the App^{NL-G-F} knock-in mouse model [29], which shows Aβ peptide accumulation, neuroinflammation, and cognitive impairment in an age-dependent manner, without the non-physiological overexpression of APP [30].

The murine App^{NL-G-F} allele has a humanized Aβ peptide sequence, owing to three amino acid substitutions (G676R, F681Y, R684H; exon 16), and harbors three familial AD mutations: Swedish (K670N, M671L; exon 16), Arctic (E693G; exon 17), and Iberian (I716F; exon 17) [29]. The lecanemab monoclonal antibody, developed as an immunotherapy and tested in recent successful clinical trials, was raised against the Arctic Aβ variant [4].

Herein, we report that spatial memory and brain metabolism deficits exhibited by 12-month-old homozygous App^{NL-G-F} mice are counteracted by the hypomorphic PDE4B, without decreasing Aβ plaque burden. This genetically mediated protective effect identifies PDE4B as a key regulator of disease manifestation in the App^{NL-G-F} model and a promising therapeutic target for AD.

METHODS AND MATERIALS
For more detailed methodology, see the Supplementary Materials and Methods.

Mice
The $Pde4b^{Y358C}$ mutation from the B6.C-$Pde4b^{enu1H}$ line [28] was bred into the C57BL/6-$App^{tm3.1(NL-G-F)Tcs}$ (App^{NL-G-F}) line [29] to generate $App^{+/+};Pde4b^{+/+}$ (wild-type; WT), $App^{NL-G-F/NL-G-F};Pde4b^{+/+}$ (App^{NL-G-F}) and $App^{NL-G-F/NL-G-F};$ $Pde4b^{Y358C/Y358C}$ ($App^{NL-G-F}/Pde4b^{Y358C}$) littermates for phenotypic testing. The mouse experiments were conducted in accordance with the UK Animals (Scientific Procedures) Act 1986 under UK Home Office licences and approved by institutional Animal Welfare and Ethical Review Bodies at the University of Leeds and Lancaster University.

Barnes maze
The Barnes maze test was conducted as described previously with slight modifications [31].

^{14}C-2-DG autoradiography
The ^{14}C-2-deoxyglucose (^{14}C-2-DG) functional brain imaging technique was undertaken as described previously [32, 33].

Inflammation assay
Cortical lysates (2.5 mg in 100 μl) were analyzed for 32 inflammatory markers in duplicate using the Mouse Cytokine/Chemokine 32-Plex Array (Eve Technologies).

Thioflavin-S staining
Aβ deposits in 4% paraformaldehyde-fixed brain sections were stained with thioflavin-S (Toronto Research Chemicals).

RNA sequencing
Sequence data from a NovaSeq 6000 (Illumina) instrument were processed using the R package DSeq2 [34] to identify differentially expressed transcripts with p-values < 0.01 adjusted (adj.) for multiple testing using the Benjamini-Hochberg false discovery rate method [35].

Western blotting
Western blotting was undertaken as previously described [31], using rabbit polyclonal antibody PC730 to insulin-degrading enzyme (IDE) (Millipore) or mouse monoclonal antibody AC-15 to β-actin (Sigma-Aldrich).

Statistical analysis
All data values in the text and figure legends are represented as the mean ± standard error of the mean. A statistically significant difference was set at $p < 0.01$ for RNA sequencing and $p < 0.05$ for other data.

RESULTS
Protective effect of hypomorphic PDE4B on spatial memory in App^{NL-G-F} mice
In the Barnes maze, App^{NL-G-F} mice previously showed deficient spatial learning and intact spatial reference memory at 8 months of age [36]. Other studies report intact spatial learning but subtly deficient spatial reference memory in App^{NL-G-F} mice aged 4.5 months [37] and 6 months [38]. We therefore aged mice to 12 months before evaluating their abilities in the Barnes maze.

Over 5 days of training, 12-month-old App^{NL-G-F} and $App^{NL-G-F}/$ $Pde4b^{Y358C}$ mice took significantly longer to reach the target hole than WT controls (primary latency; Fig. 1A). App^{NL-G-F} mice also moved more slowly on days 1–3 (velocity; Fig. S3A), took a longer path to the target hole (primary path length; Fig. 1B), and made more errors (primary errors; Fig. 1C) compared with WT controls. During the probe trial, App^{NL-G-F} mice spent less time than WT mice in the target quadrant (25% of arena) (Fig. 1D), less time than WT and $App^{NL-G-F}/Pde4b^{Y358C}$ mice in the target sector (5% of arena) (Fig. 1E), and made fewer head entries than WT and $App^{NL-G-F}/$ $Pde4b^{Y358C}$ mice into the target hole annulus (Fig. 1F). These measures were not different in $App^{NL-G-F}/Pde4b^{Y358C}$ mice relative to WT controls. Velocity was not significantly different between genotypes (Fig. S3C). App^{NL-G-F} mice thus displayed a spatial memory deficit that was prevented by the hypomorphic PDE4B present in $App^{NL-G-F}/Pde4b^{Y358C}$ mice.

Protective effect of hypomorphic PDE4B on brain metabolism in App^{NL-G-F} mice
An increasing number of studies have shown that the onset and progression of AD are closely linked to glucose hypometabolism in the brain [39]. Hence, we assessed cerebral glucose metabolism as a function of neurogenic activity in the App^{NL-G-F} model using the translational ^{14}C-2-DG brain imaging technique. In multiple brain regions, including the stratum lacunosum-moleculare (SLM) in hippocampal CA1 and subfields of the prefrontal cortex (PFC), glucose utilization was significantly lower in 13-month-old App^{NL-G-F} mice than in WT controls. However, significantly increased glucose utilization was observed in $App^{NL-G-F}/Pde4b^{Y358C}$ relative to App^{NL-G-F} mice in many of these regions, with cerebral metabolism being restored to the same level as that observed in WT controls (Fig. 2A–F). Aside from the SLM, glucose utilization in the hippocampus was not significantly different in App^{NL-G-F} and $App^{NL-G-F}/Pde4b^{Y358C}$ mice relative to WT controls, although a significant increase in hippocampal metabolism was observed in $App^{NL-G-F}/Pde4b^{Y358C}$ versus App^{NL-G-F} mice (Fig. 2G, H). Exemplar color-coded autoradiographs of coronal brain sections are shown in Fig. 3. Full data are shown in Tables S1 & S2. App^{NL-G-F} mice thus displayed a widespread cerebral hypometabolism that was prevented by the hypomorphic PDE4B present in $App^{NL-G-F}/$ $Pde4b^{Y358C}$ mice.

Since Aβ deposition in cerebral gray matter is one of the hallmark pathologies of AD [1], we evaluated whether the Aβ plaque burden in 12-month-old App^{NL-G-F} mice was affected by hypomorphic PDE4B. The percentage of surface area occupied by thioflavin-S-stained Aβ plaques was not significantly different between App^{NL-G-F} and $App^{NL-G-F}/Pde4b^{Y358C}$ mice (Fig. S4).

Partial attenuation of neuroinflammation in App^{NL-G-F} mice by hypomorphic PDE4B
The involvement of neuroinflammation in AD is supported by accumulating evidence, including the manifestation of microgliosis in App^{NL-G-F} mice from 9 months of age [29, 40]. As PDE4B is the predominant negative modulator of cAMP signaling in microglia [41], which release elevated levels of inflammatory markers when chronically activated [42], we evaluated the brain levels of 32 inflammatory markers in 12-month-old mice. Brain lysates from App^{NL-G-F} mice showed increased levels of three cytokines (IFNγ, LIF & M-CSF; Fig. S5), four chemokines (IP-10, MIG,
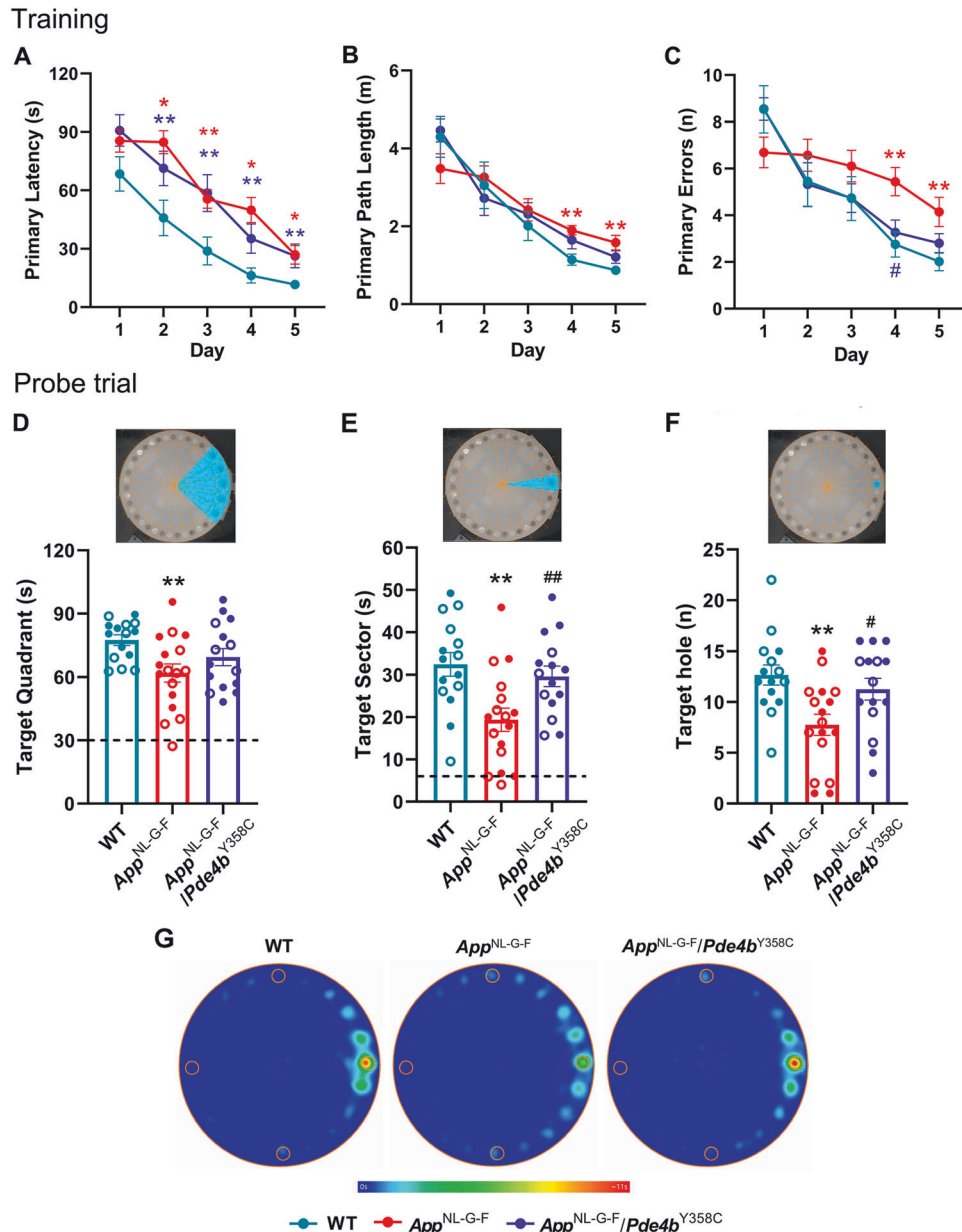
Training

Probe trial

Fig. 1 Protective effect of hypomorphic PDE4B on spatial memory in App^{NL-G-F} mice assessed by the Barnes maze. A Primary latency (s). All three genotypes showed a significant decrease over the five training days (Friedman's ANOVA, WT: $\chi^2_4 = 37.819$, $p < 0.001$; App^{NL-G-F}: $\chi^2_4 = 39.847$, $p < 0.001$; $App^{NL-G-F}/Pde4b^{Y358C}$: $\chi^2_4 = 43.518$, $p < 0.001$). Genotypic differences were observed from day 2 (Kruskal-Wallis test, day 2: $\chi^2_2 = 8.939$, $p = 0.011$; day 3: $\chi^2_2 = 10.142$, $p = 0.006$; day 4: $\chi^2_2 = 15.830$, $p < 0.001$; day 5: $\chi^2_2 = 10.712$, $p = 0.005$). **B** Primary path length (m). All three genotypes showed a significant decrease over the five training days (Friedman's ANOVA, WT: $\chi^2_4 = 34.880$, $p < 0.001$; App^{NL-G-F}: $\chi^2_4 = 27.6^2_4$, $p < 0.001$; $App^{NL-G-F}/Pde4b^{Y358C}$: $\chi^2_4 = 37.867$, $p < 0.001$). Genotypic differences were observed on days 4 and 5 (Kruskal-Wallis test, day 4: $\chi^2_2 = 10.078$, $p = 0.006$; day 5: $\chi^2_2 = 9.441$, $p = 0.009$). **C** Number of errors. All three genotypes showed a significant decrease over the five training days (Friedman's ANOVA, WT: $\chi^2_4 = 26.726$, $p < 0.001$; App^{NL-G-F}: $\chi^2_4 = 15.075$, $p = 0.005$; $App^{NL-G-F}/Pde4b^{Y358C}$: $\chi^2_4 = 34.562$, $p < 0.001$). Genotypic differences were observed on days 4 and 5 (Kruskal-Wallis test, day 4: $\chi^2_2 = 11.461$, $p = 0.003$; day 5: $\chi^2_2 = 7.209$, $p = 0.027$). **D** Time (s) spent in target quadrant. Genotypic differences were observed (ANOVA, $F_{2,41} = 4.304$, $p = 0.02$). **E** Time (s) spent in target sector. Genotypic differences were observed (ANOVA, $F_{2,41} = 6.111$, $p = 0.005$). **F** Number of head entries into the target hole annulus. Genotypic differences were observed (ANOVA, $F_{2,41} = 5.547$, $p = 0.007$). **G** Heat maps showing the cumulative time spent in localities of the arena. 12-month-old WT ($n = 15$), App^{NL-G-F} ($n = 17$) and $App^{NL-G-F}/Pde4b^{Y358C}$ ($n = 15$) mice. Data are plotted as mean ± SEM. *$p < 0.05$; **$p < 0.01$ vs. WT. #$p < 0.05$; ##$p < 0.01$ vs. App^{NL-G-F}. Open circles, females; closed circles, males; broken line, chance level.

MIP-1α & MIP-1β), and one growth factor (VEGF-A; Fig. S6) compared with WT lysates (Fig. 4A). The levels of five of these markers (IFNγ, LIF, M-CSF, IP-10 & VEGF-A) were significantly decreased in $App^{NL-G-F}/Pde4b^{Y358C}$ compared with App^{NL-G-F} lysates (Figs. S5 and S6), reflected by lower Z scores for cytokines (Fig. 4B), chemokines (Fig. 4C), growth factors (Fig. 4D) and all 32 markers (Fig. 4E). App^{NL-G-F} mice thus displayed neuroinflammation that

was partially attenuated by the hypomorphic PDE4B present in $App^{NL-G-F}/Pde4b^{Y358C}$ mice. Lysates from $App^{NL-G-F}/Pde4b^{Y358C}$ mice also showed significantly decreased levels of IL-9 (Fig. S5K), eotaxin (Fig. S6A), and LIX (Fig. S6C) compared with WT lysates, suggesting additional anti-inflammatory effects of PDE4B inhibition in the brains of 12-month-old mice independent of App genotype.
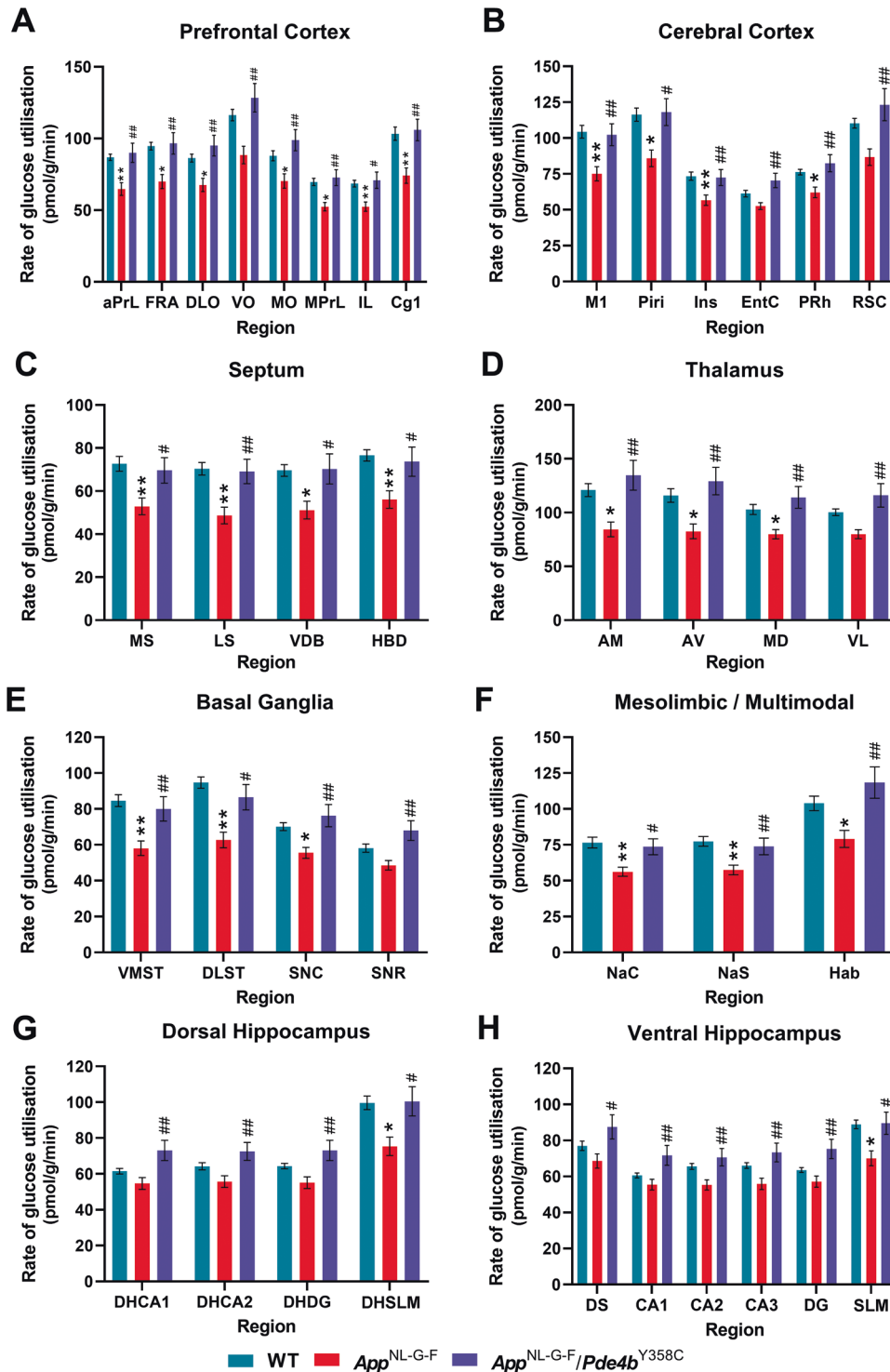
Fig. 2 Protective effect of hypomorphic PDE4B on brain metabolism in App^{NL-G-F} mice assessed by ^{14}C-2-DG brain imaging. App^{NL-G-F} mice show hypometabolism that is corrected in App^{NL-G-F}/Pde4b^{Y358C} mice in multiple subfields of the PFC (**A**), cerebral cortex (**B**), septum (**C**), thalamus (**D**), basal ganglia (**E**), and mesolimbic pathway (**F**). App^{NL-G-F} also show hypometabolism selectively in the DHSLM and SLM that was corrected in App^{NL-G-F}/Pde4b^{Y358C} mice (**G**, **H**). In other hippocampal subfields, App^{NL-G-F} mice did not show hypometabolism, whereas metabolism was enhanced in these subfields in App^{NL-G-F}/Pde4b^{Y358C} mice. 13-month-old WT ($n = 15$), App^{NL-G-F} ($n = 17$) and App^{NL-G-F}/Pde4b^{Y358C} ($n = 15$) mice. Data are plotted as mean ± SEM. Student's t-test with Bonferonni-Holm post hoc correction for multiple comparisons. *$p < 0.05$; **$p < 0.01$ vs. WT. #$p < 0.05$; ##$p < 0.01$ vs. App^{NL-G-F}. Brain region abbreviations are defined in Table S1.

Modulation of differentially expressed genes in App^{NL-G-F} mice by hypomorphic PDE4B

As PDE4B regulates cAMP gradients and ultimately the transcription factor CREB [43], we performed transcriptomic analysis (RNA sequencing) on cerebral cortical tissue from 12-month-old mice to identify molecular pathways potentially underlying the protective effect of PDE4B inhibition in App^{NL-G-F} mouse brain. Among 76,076 gene transcripts that were robustly expressed, 531
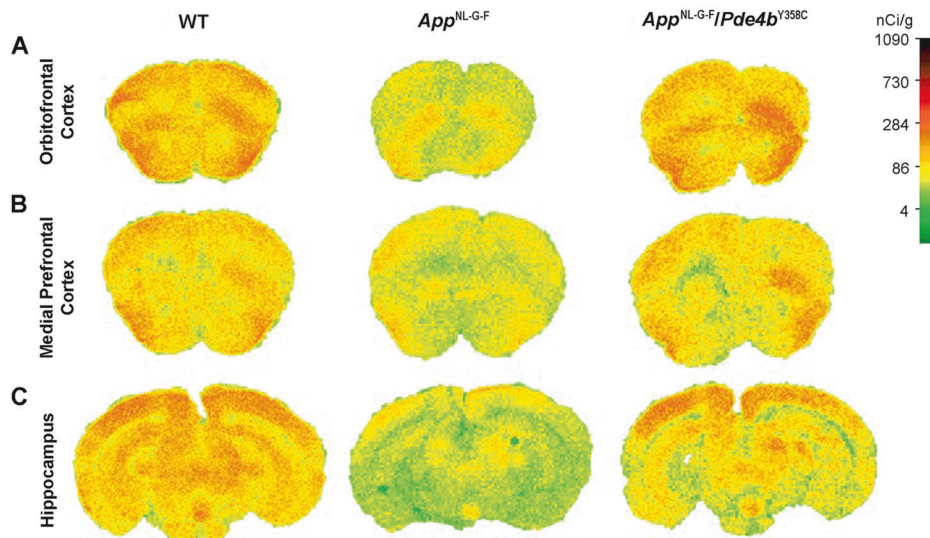
Fig. 3 Exemplar ¹⁴C-2-DG color-coded autoradiographs obtained from coronal brain sections of 13-month-old WT, App^NL-G-F, and App^NL-G-F/ Pde4b^Y358C mice. A Orbitofrontal cortex ($+2.46$ mm from bregma). **B** Medial PFC ($+1.98$ mm from bregma). **C** Hippocampus (-3.16 mm from bregma). Higher rates of metabolism are indicated by red/orange and lower rates indicated by yellow/white. Scale bar indicates tissue ¹⁴C concentration (nCi/g).

were differentially expressed (DE) at an adjusted significance threshold of $p < 0.01$ in App^NL-G-F (527 up, 4 down) (Fig. S7A; Table S3) and 462 were DE in App^NL-G-F/Pde4b^Y358C (379 up, 83 down) (Fig. S7B; Table S4) versus WT mice. The number of DE transcripts in App^NL-G-F/Pde4b^Y358C versus App^NL-G-F mice was 117 (21 up, 96 down) (Fig. S7C; Table S5).

Among the 531 transcripts DE in App^NL-G-F mice, 314 were also DE in App^NL-G-F/Pde4b^Y358C versus WT but not significantly different between App^NL-G-F and App^NL-G-F/Pde4b^Y358C (Table S6), suggesting transcriptional effects of the App^NL-G-F allele that were not significantly affected by hypomorphic PDE4B. Included in them are CCl3 (1 up) encoding MIP-1α (Fig. S8A), corroborating the inflammatory marker assay result, as well as Itgax (4 up) (Fig. S8B), a marker of disease-associated microglia (DAM) activation, and Gfap (4 up) (Fig. S8C), a marker of astrocyte activation (reactive astrogliosis).

Among the remaining 217 transcripts DE in App^NL-G-F mice, all but one (C1qb) were not significantly different between App^NL-G-F/ Pde4b^Y358C and WT mice (Table S7). Included in them is Cxcl5 (1 up) encoding LIX (Fig. S8D), as well as the DAM activation markers Fth1 (2 up) (Fig. S8E) and Mamdc2 (4 up) (Fig. S8F), and the reactive astrocyte markers Dbi (2 up), Aqp4 (9 up), Ifitm3 (1 up) and Osmr (6 up) (Fig. S8G–J). Hypomorphic PDE4B had the greatest modulatory effect on 13 transcripts (from four genes), as they were significantly different between App^NL-G-F/Pde4b^Y358C and App^NL-G-F mice (blue dots, Fig. S7C; Table S8). These most modulated transcripts include Ide (7 up from 7) (Fig. 5A), Btaf1 (3 up from 5) (Fig. 5B), and Padi2 (2 up from 2) (Fig. 5C), whose expression was normalized by the hypomorphic PDE4B present in App^NL-G-F/Pde4b^Y358C mice. Also included is C1qb (1 up from 1) (Fig. 5D), a marker of homeostatic microglia, which was significantly different between App^NL-G-F/Pde4b^Y358C and WT mice, indicating a milder modulatory effect of the PDE4B hypomorph. App^NL-G-F mice thus displayed gene expression differences that were modulated by the hypomorphic PDE4B present in App^NL-G-F/ Pde4b^Y358C mice.

Among the 75,545 transcripts that were not DE in App^NL-G-F versus WT mice, 41 were DE in App^NL-G-F/Pde4b^Y358C (14 up, 27 down) versus both WT and App^NL-G-F mice (Table S9). App^NL-G-F/ Pde4b^Y358C mice thus displayed gene expression differences driven by hypomorphic PDE4B that were not significantly affected by the App^NL-G-F allele (e.g., Casp9 and Nr1d1; Fig. S8K, L). A further

106 transcripts were DE in App^NL-G-F/Pde4b^Y358C (55 up, 51 down) versus WT but not versus App^NL-G-F mice (Table S9), suggesting modulation by the App^NL-G-F allele of PDE4B hypomorph-driven gene expression differences (e.g., Per2; Fig. S8M).

As increased levels of IDE (insulysin), encoded by Ide, have been observed in brain tissue from 9–18-month-old APPswe/PSEN1dE9 [44, 45] and Tg2576 [46] transgenic mice that overexpress human Swedish mutant APP, we quantified the amount of IDE in brain lysates from 12-month-old mice by western blotting. Consistent with the RNA sequencing results, the level of IDE was upregulated in App^NL-G-F versus WT mice, but this upregulation was blunted in App^NL-G-F/Pde4b^Y358C lysates (Fig. 5E, F), confirming a modulating effect of hypomorphic PDE4B on IDE expression. Correlation coefficients revealed positive correlations between brain levels of IDE and inflammatory marker Z scores across all genotypes (Fig. S9), indicating that higher levels of IDE were associated with greater inflammation.

DISCUSSION

Authentic animal models serve as valuable tools for determining the molecular mechanisms of disease progression and testing potential therapeutic approaches. The App^NL-G-F model develops Aβ plaques, neuroinflammation, damaged synapses, and behavioral and cognitive deficits, while accurately recapitulating endogenous APP expression [29, 30]. However, it was unknown whether App^NL-G-F mice also replicate the cerebral hypometabolism that is a hallmark feature of AD [39]. Accumulating studies have shown that this decline in cerebral glucose metabolism occurs before pathology and symptoms manifest, continues as symptoms progress, and is more severe than the gradual decline in metabolic efficiency during normal aging [47]. 18-fluorodeoxyglucose positron emission tomography (PET) brain imaging in AD patients has observed cerebral glucose metabolism deficits in a range of brain regions, including the PFC and medial temporal lobe/hippocampus [48, 49], with this hypometabolism being a potentially useful diagnostic biomarker [50].

Using the translational ¹⁴C-2-DG brain imaging technique, we observed that 13-month-old App^NL-G-F mice exhibit widespread glucose hypometabolism in multiple brain regions, which was prevented by the hypomorphic PDE4B present in App^NL-G-F/ Pde4b^Y358C mice. Glucose utilization was highest in the thalamus,
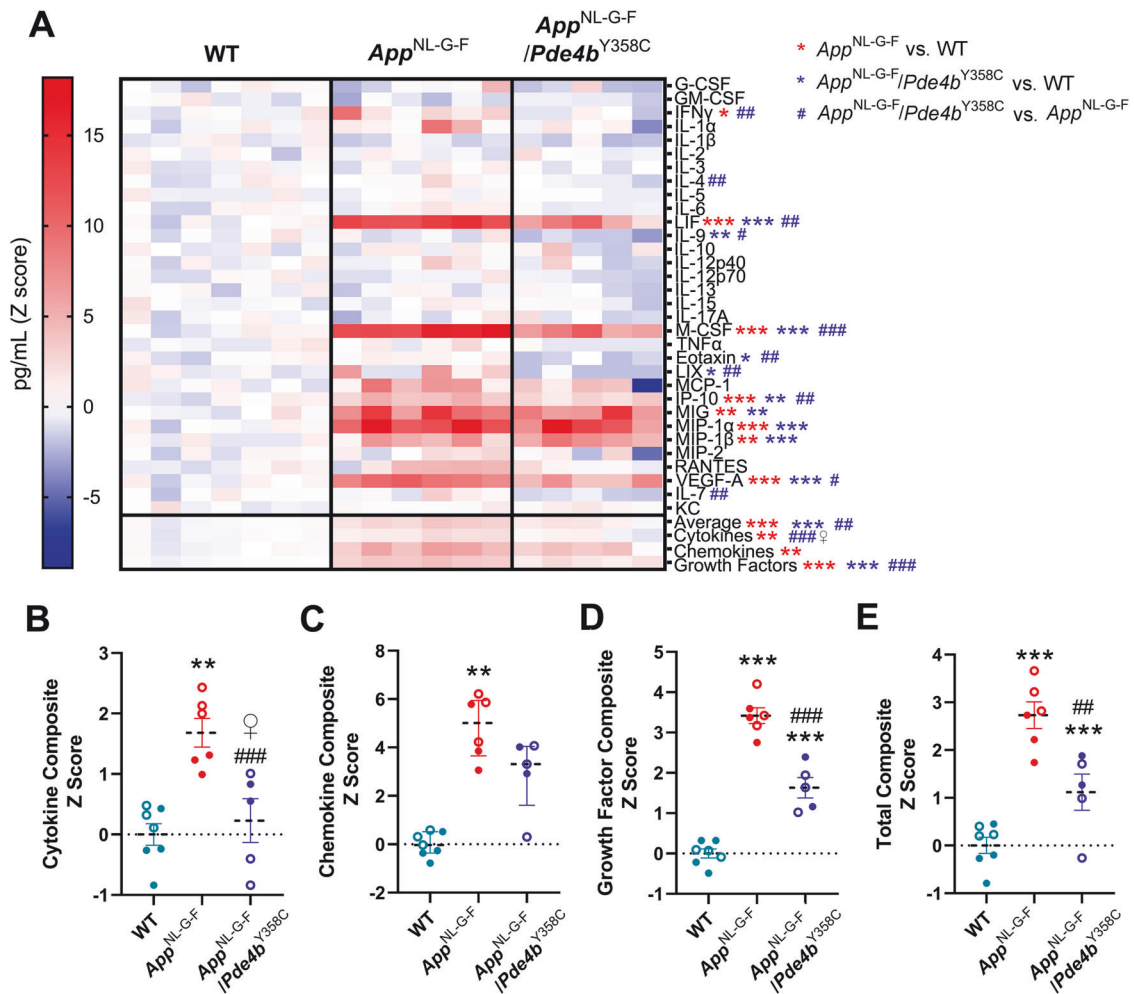
Fig. 4 Partial attenuation of neuroinflammation in App^{NL-G-F} mice by hypomorphic PDE4B. A Heatmap analysis of Z scores of 32 inflammatory markers, each column indicating a different mouse. App^{NL-G-F} mice show elevated levels of inflammatory markers, which are partly decreased in $App^{NL-G-F}/Pde4b^{Y358C}$ mice. Composite Z scores for cytokines (**B**), chemokines (**C**), growth factors (**D**), and all 32 markers (total; **E**) are elevated in App^{NL-G-F} mice but modulated by the PDE4B inhibition in $App^{NL-G-F}/Pde4b^{Y358C}$ mice. 12-month-old WT ($n = 7$), App^{NL-G-F} ($n = 6$) and $App^{NL-G-F}/Pde4b^{Y358C}$ ($n = 5$) mice. Data are plotted as mean ± SEM. *$p < 0.05$; **$p < 0.01$; ***$p < 0.001$ vs. WT. #$p < 0.05$; ##$p < 0.01$; ###$p < 0.001$ vs. App^{NL-G-F}. Open circles, females; closed circles, males; ♀, significant difference in females only.

consistent with the distribution of PDE4B in the primate brain [51, 52]. Targeted inhibition of PDE4B is thus an intervention that increases cerebral metabolism in App^{NL-G-F} mice (i.e., improves the neuronal energy state) and therefore has the potential to be disease-modifying in patients. By contrast, acute pretreatment of normal mice and rats with the pan-PDE4 inhibitor rolipram decreases glucose utilization in brain tissue [53–56]. Moreover, pan-PDE4 inhibitors have dose-dependent side effects of nausea and emesis – attributed to the selective inhibition of PDE4D – which limit their tolerability and translational value [57].

The SLM serves as a relay between the entorhinal cortex (EC) and the CA1 and is believed to represent the substrate of distinct aspects of spatial and episodic memory [58, 59]. Neurons of the EC that send projections to the CA1 are the initial degenerating cells in AD [60]. Considering the spatial memory impairment of App^{NL-G-F} mice, it is noteworthy that their hippocampal hypometabolism was restricted to the SLM. However, App^{NL-G-F} mice also exhibited hypometabolism in the PFC, which itself has a role in spatial memory formation [61, 62]. The restoration of glucose metabolism in both the SLM and PFC thus likely contributed to the improved spatial memory of $App^{NL-G-F}/Pde4b^{Y358C}$ mice.

Cerebral glucose hypometabolism has previously been observed in transgenic APP-overexpressing mouse models of AD. The PDAPP

strain showed glucose hypometabolism across multiple brain regions at 10 months of age [63], but this reached statistical significance only in the posterior cingulate cortex in 17-month-old mice following Bonferroni correction for multiple comparisons [64]. The PS/APP strain had localized hypometabolism in several brain regions but an unaltered whole brain average at 16 months [65], whereas the 3xTg-AD strain showed widespread hypometabolism in all measured brain regions at 18 months of age [66].

The area occupied by thioflavin-S-stained Aβ plaques in brain sections from 12-month-old App^{NL-G-F} mice was similar to that previously reported for 11-month-old App^{NL-G-F} mice, which showed a mild corticolimbic Aβ pathology relative to age-matched 5xFAD and APPswe/PSEN1dE9 mice that overexpress APP [67]. The similar Aβ plaque burdens of App^{NL-G-F} and $App^{NL-G-F}/Pde4b^{Y358C}$ mice in the present study suggest that a decrease in Aβ plaque load is not responsible for the prevention of spatial memory and brain metabolism deficits by hypomorphic PDE4B. The situation in $App^{NL-G-F}/Pde4b^{Y358C}$ mice is thus comparable with that of the ~30% of older adults without signs of cognitive impairment who exhibit the neuropathological features of AD upon autopsy at the time of death [68]. This is not, however, contradictory to PDE4B being a promising therapeutic target for AD. There is a need for non-Aβ-directed therapies for AD because Aβ-targeting antibodies
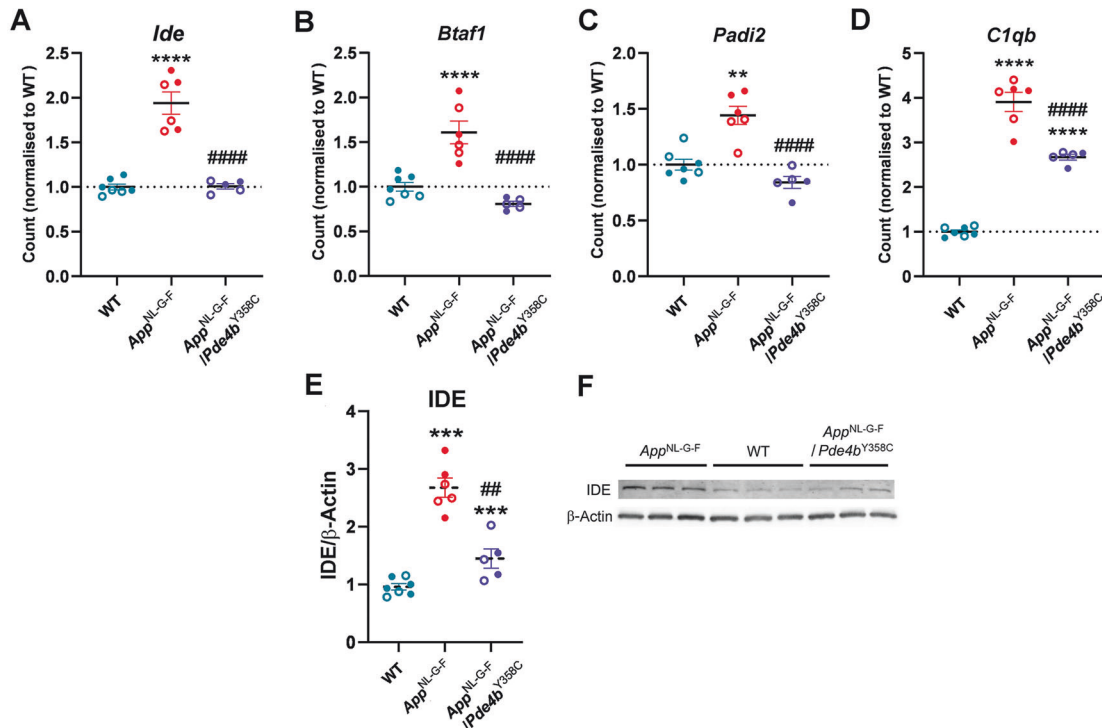
Fig. 5 Modulation of differentially expressed cerebral cortical genes in App^{NL-G-F} mice by hypomorphic PDE4B. A *Ide* (mean of 7 transcripts). **B** *Btaf1* (mean of 3 transcripts). **C** *Padi2* (mean of 2 transcripts). **D** *C1qb* (1 transcript). **E** Immunoreactivity of IDE protein normalized to β-Actin in brains. Genotypic differences were observed (Kruskal-Wallis test, $\chi^2_{18} = 14.259$, $p = 0.001$). **F** Typical blot of 50 μg protein from brains probed with anti-IDE and anti-β-Actin antibodies. 12-month-old WT ($n = 7$), App^{NL-G-F} ($n = 6$) and $App^{NL-G-F}/Pde4b^{Y358C}$ ($n = 5$) mice. Data are plotted as mean ± SEM. **adj. $p < 0.01$, ****adj. $p < 0.0001$ vs. WT; ####adj. $p < 0.0001$ vs. App^{NL-G-F} for **A**–**D**. ***$p < 0.001$ vs. WT; ##$p < 0.01$ vs. App^{NL-G-F} for (**E**).

have shown only modest cognitive benefit in early AD [4, 5], and more than 20% of individuals diagnosed with AD do not have Aβ plaque burden as assessed by PET imaging [69].

Despite the central role of PDE4B in inflammation [70–72], the upregulation of multiple inflammatory markers in both $App^{NL-G-F}/Pde4b^{Y358C}$ and App^{NL-G-F} mice suggests that the protective effect of hypomorphic PDE4B cannot be attributed to a broad anti-inflammatory response. Although TNFα levels were not significantly affected by genotype, the lack of detectable TNFα in four of the five $App^{NL-G-F}/Pde4b^{Y358C}$ mice is consistent with the known suppression of TNFα production by PDE4B ablation and selective inhibition [72, 73].

RNA sequencing to identify molecular pathways potentially underlying the protective effect of hypomorphic PDE4B revealed that 531 of 76,076 robustly expressed gene transcripts were DE in cerebral cortical tissue from App^{NL-G-F} versus WT mice. None of the PDE4 transcripts (*Pde4a–d*) were DE in App^{NL-G-F} mice (Table S10), unlike the upregulation of *Pde4b* in cultured microglia exposed to Aβ peptides [11]. Among APP-overexpressing mouse models, the 3xTg-AD strain exhibited increased PDE4B and PDE4D protein levels in hippocampus and PFC, which were decreased by rolipram [22], and the APPswe/PSEN1dE9 strain exhibited increased PDE4B and PDE4D protein levels in cerebral cortex, which were decreased by roflumilast [24].

Among the transcripts DE in App^{NL-G-F} mice, 59% were also DE in $App^{NL-G-F}/Pde4b^{Y358C}$ versus WT mice, including the upregulation of *CCl3*, encoding MIP-1α that was also upregulated in the inflammatory marker assay. None of the *Pde4b* transcripts (0 of 9) were DE in $App^{NL-G-F}/Pde4b^{Y358C}$ versus WT mice (Table S10), as expected from prior analyses of $Pde4b^{Y358C}$ mouse brain tissue [28]. Both increased and decreased expression of *Pde4b* in the hippocampus have been shown to impair contextual fear memory in mice [74].

Remarkably, the levels of only 13 of the DE transcripts – from four genes: *Ide*, *Btaf1*, *Padi2*, and *C1qb* – were significantly different

between $App^{NL-G-F}/Pde4b^{Y358C}$ and App^{NL-G-F} mice, suggesting that their expression was the most modulated by the hypomorphic PDE4B. The 13 include all *Ide* (7 of 7), *Padi2* (2 of 2), and *C1qb* (1 of 1) transcripts, but only three of the five *Btaf1* transcripts in the RNA sequence dataset. Multiple independent transcripts thus provide support for three of these genes at the conservative adjusted significance threshold employed ($p < 0.01$), but we cannot exclude the possibility that the single transcript representing *C1qb* is a false positive.

Padi2, encoding protein-arginine deiminase type-2 (PADI2) that converts arginine residues in proteins into citrullines (citrullination) through deamination [75], and *Ide*, encoding a ubiquitously expressed metalloprotease (IDE) that cleaves peptides including Aβ [76, 77], are noteworthy because their expression is upregulated in postmortem AD patient brains compared with age-matched controls. Markedly increased levels of PADI2 are detected in hippocampal samples from AD patients, and the immunoreactivity of PADI2 and citrullinated proteins coincides with glial fibrillary acidic protein (GFAP)-positive astrocytes [78]. Increased levels of IDE are detected in postmortem brains from patients with moderate AD pathology (Braak stages III–IV) although decreased levels of IDE are found in severe AD (Braak stages V–VI) [79].

IDE levels in cerebral cortex from 9-month-old APPswe/PSEN1dE9 mice are elevated after the formation of the first Aβ plaques and show a positive correlation with full-length APP levels [44]. In 10- and 18-month-old APPswe/PSEN1dE9 mice, the expression of IDE is inversely correlated with spatial memory in the Morris water maze [45]. In 16-month-old Tg2576 mice, increased IDE expression appears within GFAP-positive astrocytes surrounding Aβ plaques [46]. Like these transgenic APP-overexpressing strains, 12-month-old App^{NL-G-F} mice, but not $App^{NL-G-F}/Pde4b^{Y358C}$ mice, show upregulation of IDE protein in the

brain – conceivably representing a compensatory mechanism aimed to decrease Aβ, MIP-1α, and MIP-1β levels. Despite the involvement of GFAP-positive astrocytes in the expression of *Padi2* and *Ide*, this cell type is unlikely to mediate the modulation of these transcripts by PDE4B inhibition because *Gfap* was upregulated in both App^{NL-G-F} and $App^{NL-G-F}/Pde4b^{Y358C}$ mice. However, the upregulation of some less abundant reactive astrocyte markers, such as *Aqp4*, was blunted in $App^{NL-G-F}/Pde4b^{Y358C}$ mice.

The normalization of IDE expression in $App^{NL-G-F}/Pde4b^{Y358C}$ mice suggests that activation of the cAMP signaling pathway negatively regulates IDE expression. This observation is consistent with the finding that IDE expression in streptozotocin-treated APPswe/PSEN1dE9 mice is decreased by administration of the cAMP analog and non-subtype-selective cAMP phosphodiesterase inhibitor bucladesine in a dose-dependent manner [80]. The convergence between our observations in App^{NL-G-F} mice and published findings from transgenic mice that overexpress APP suggest that cerebral hypometabolism and IDE upregulation are not artifacts related to the non-physiological overproduction of various APP fragments in the APP-overexpressing strains [30].

Although we have identified that the $Pde4b^{Y358C}$ hypomorph corrected expression changes of specific cortical transcripts but did not decrease Aβ plaque burden in App^{NL-G-F} mice, a limitation of this study is that it has not elucidated the mechanism underlying the protective effect of hypomorphic PDE4B in the App^{NL-G-F} model. Since we aimed to evaluate the neurocognitive effects of genetically inhibiting PDE4B in App^{NL-G-F} mice, the study did not include a group with the $Pde4b^{Y358C}$ mutation on a WT ($App^{+/+}$) background. Previous studies have employed similar experimental designs without a treatment-only $App^{+/+}$ group to assess the effects of genetic modifications in App^{NL-G-F} mice [81–83]. However, the lack of a $Pde4b^{Y358C}$-only group precluded statistical analysis of *Pde4b* genotype as an independent variable. Consequently, an additional limitation is that we could not evaluate the effect of PDE4B inhibition in 12-month-old mice independently of the App^{NL-G-F} mutant allele. Another limitation is that the App^{NL-G-F} model does not exhibit tau-containing neurofibrillary tangles, a histopathological hallmark of AD [29, 30]. Rolipram suppresses tau phosphorylation in 11-month-old 3xTg-AD mice [22] and in the rTg4510 mouse model of frontotemporal dementia at 3–4 months of age [84], but no work has been published on the effects of PDE4B subtype-specific inhibition on tau pathology. A further limitation is that the B6.C-$Pde4b^{enu1H}$ mouse line employed does not permit spatial or temporal control over expression of the $Pde4b^{Y358C}$ mutation. A $Pde4b^{Y358C}$ conditional knock-in line would allow us to test whether hypomorphic PDE4B can arrest or reverse progression at different stages of disease in the App^{NL-G-F} model.

In summation, our data show that App^{NL-G-F} mice exhibit spatial memory and brain metabolism deficits that are prevented by targeted inhibition of PDE4B, a cAMP hydrolyzing enzyme that has been implicated in the pathogenesis of AD by a recent meta-analysis of GWAS data [7]. To the best of our knowledge, this is the first study demonstrating that PDE4B subtype-specific inhibition has a protective effect in a preclinical model of AD. This novel finding identifies the PDE4B subtype as a key regulator of disease manifestation in the App^{NL-G-F} model and a promising therapeutic target for AD.

REFERENCES

1. Tarawneh R, Holtzman DM. The clinical problem of symptomatic Alzheimer disease and mild cognitive impairment. Cold Spring Harb Perspect Med. 2012;2:a006148.
2. Gatz M, Reynolds CA, Fratiglioni L, Johansson B, Mortimer JA, Berg S, et al. Role of genes and environments for explaining Alzheimer disease. Arch Gen Psychiatry. 2006;63:168–74.
3. Polderman TJ, Benyamin B, de Leeuw CA, Sullivan PF, van Bochoven A, Visscher PM, et al. Meta-analysis of the heritability of human traits based on fifty years of twin studies. Nat Genet. 2015;47:702–9.
4. van Dyck CH, Swanson CJ, Aisen P, Bateman RJ, Chen C, Gee M, et al. Lecanemab in early Alzheimer's disease. N Engl J Med. 2023;388:9–21.
5. Sims JR, Zimmer JA, Evans CD, Lu M, Ardayfio P, Sparks J, et al. Donanemab in early symptomatic Alzheimer disease: the TRAILBLAZER-ALZ 2 randomized clinical trial. JAMA. 2023;330:512–27.
6. Gau SY, Lai JN, Yip HT, Wu MC, Wei JC. Higher dementia risk in people with gastroesophageal reflux disease: a real-world evidence. Front Aging Neurosci. 2022;14:830729.
7. Adewuyi EO, O'Brien EK, Nyholt DR, Porter T, Laws SM. A large-scale genome-wide cross-trait analysis reveals shared genetic architecture between Alzheimer's disease and gastrointestinal tract disorders. Commun Biol. 2022;5:691.
8. Bunnage ME, Gilbert AM, Jones LH, Hett EC. Know your target, know your molecule. Nat Chem Biol. 2015;11:368–72.
9. Yao Z, van Velthoven CTJ, Nguyen TN, Goldy J, Sedeno-Cortes AE, Baftizadeh F, et al. A taxonomy of transcriptomic cell types across the isocortex and hippocampal formation. Cell. 2021;184:3222–41.e26.
10. Bakken TE, Jorstad NL, Hu Q, Lake BB, Tian W, Kalmbach BE, et al. Comparative cellular analysis of motor cortex in human, marmoset and mouse. Nature. 2021;598:111–9.
11. Sebastiani G, Morissette C, Lacagé C, Boulé M, Ouellette MJ, McLaughlin RW, et al. The cAMP-specific phosphodiesterase 4B mediates Abeta-induced microglial activation. Neurobiol Aging. 2006;27:691–701.
12. Bales KR, Plath N, Svenstrup N, Menniti FS. Phosphodiesterase inhibition to target the synaptic dysfunction in Alzheimer's disease. In: Dominguez C, editor. Neurodegenerative diseases. Topics in medicinal chemistry. Vol. 6; Berlin, Heidelberg: Springer; 2010. pp. 57–90.
13. García-Osta A, Cuadrado-Tejedor M, García-Barroso C, Oyarzábal J, Franco R. Phosphodiesterases as therapeutic targets for Alzheimer's disease. ACS Chem Neurosci. 2012;3:832–44.
14. Kametani F. Phosphodiesterase as a drug target of Alzheimer's disease. Austin Alzheimers J Parkinsons Dis. 2015;2:1021.
15. Wu Y, Li Z, Huang YY, Wu D, Luo HB. Novel phosphodiesterase inhibitors for cognitive improvement in Alzheimer's disease. J Med Chem. 2018;61:5467–83.
16. Nabavi SM, Talarek S, Listos J, Nabavi SF, Devi KP, Roberto de Oliveira M, et al. Phosphodiesterase inhibitors say NO to Alzheimer's disease. Food Chem Toxicol. 2019;134:110822.
17. Tibbo AJ, Tejeda GS, Baillie GS. Understanding PDE4's function in Alzheimer's disease; a target for novel therapeutic approaches. Biochem Soc Trans. 2019;47:1557–65.
18. Sanders O, Rajagopal L. Phosphodiesterase inhibitors for Alzheimer's disease: a systematic review of clinical trials and epidemiology with a mechanistic rationale. J Alzheimers Dis Rep. 2020;4:185–215.
19. Xi M, Sun T, Chai S, Xie M, Chen S, Deng L, et al. Therapeutic potential of phosphodiesterase inhibitors for cognitive amelioration in Alzheimer's disease. Eur J Med Chem. 2022;232:114170.
20. Gong B, Vitolo OV, Trinchese F, Liu S, Shelanski M, Arancio O. Persistent improvement in synaptic and cognitive functions in an Alzheimer mouse model after rolipram treatment. J Clin Invest. 2004;114:1624–34.
21. Comery TA, Martone RL, Aschmies S, Atchison KP, Diamantidis G, Gong X, et al. Acute gamma-secretase inhibition improves contextual fear conditioning in the Tg2576 mouse model of Alzheimer's disease. J Neurosci. 2005;25:8898–902.
22. Cong YF, Liu FW, Xu L, Song SS, Shen XR, Liu D, et al. Rolipram ameliorates memory deficits and depression-like behavior in APP/PS1/tau triple transgenic mice: involvement of neuroinflammation and apoptosis via cAMP signaling. Int J Neuropsychopharmacol. 2023;26:585–98.
23. Feng H, Wang C, He W, Wu X, Li S, Zeng Z, et al. Roflumilast ameliorates cognitive impairment in APP/PS1 mice via cAMP/CREB/BDNF signaling and anti-neuroinflammatory effects. Metab Brain Dis. 2019;34:583–91.
24. Wang H, Zhang FF, Xu Y, Fu HR, Wang XD, Wang L, et al. The phosphodiesterase-4 inhibitor roflumilast, a potential treatment for the comorbidity of memory loss and depression in Alzheimer's disease: a preclinical study in APP/PS1 transgenic mice. Int J Neuropsychopharmacol. 2020;23:700–11.
25. Guo H, Cheng Y, Wang C, Wu J, Zou Z, Niu B, et al. FFPM, a PDE4 inhibitor, reverses learning and memory deficits in APP/PS1 transgenic mice via cAMP/PKA/CREB signaling and anti-inflammatory effects. Neuropharmacology. 2017;116:260–9.
26. Sierksma AS, van den Hove DL, Pfau F, Philippens M, Bruno O, Fedele E, et al. Improvement of spatial memory function in APPswe/PS1dE9 mice after chronic inhibition of phosphodiesterase type 4D. Neuropharmacology. 2014;77:120–30.
27. Ricciarelli R, Brullo C, Prickaerts J, Arancio O, Villa C, Rebosio C, et al. Memory-enhancing effects of GEBR-32a, a new PDE4D inhibitor holding promise for the treatment of Alzheimer's disease. Sci Rep. 2017;7:46320.
28. McGirr A, Lipina TV, Mun HS, Georgiou J, Al-Amri AH, Ng E, et al. Specific inhibition of phosphodiesterase-4B results in anxiolysis and facilitates memory acquisition. Neuropsychopharmacology. 2016;41:1080–92.

29. Saito T, Matsuba Y, Mihira N, Takano J, Nilsson P, Itohara S, et al. Single App knock-in mouse models of Alzheimer's disease. Nat Neurosci. 2014;17:661–3.

30. Sasaguri H, Hashimoto S, Watamura N, Sato K, Takamura R, Nagata K, et al. Recent advances in the modeling of Alzheimer's disease. Front Neurosci. 2022; 16:807473.

31. Al-Amri AH, Armstrong P, Amici M, Ligneul C, Rouse J, El-Asrag ME, et al. PDZD8 disruption causes cognitive impairment in humans, mice, and fruit flies. Biol Psychiatry. 2022;92:323–34.

32. Dawson N, Ferrington L, Lesch KP, Kelly PA. Cerebral metabolic responses to 5-HT2A/C receptor activation in mice with genetically modified serotonin transporter (SERT) expression. Eur Neuropsychopharmacol. 2011;21:117–28.

33. Hughes RB, Whittingham-Dowd J, Clapcote SJ, Broughton SJ, Dawson N. Altered medial prefrontal cortex and dorsal raphé activity predict genotype and correlate with abnormal learning behavior in a mouse model of autism-associated 2p16.3 deletion. Autism Res. 2022;15:614–27.

34. Love MI, Huber W, Anders S. Moderated estimation of fold change and dispersion for RNA-seq data with DESeq2. Genome Biol. 2014;15:550.

35. Benjamini Y, Hochberg Y. Controlling the false discovery rate: a practical and powerful approach to multiple testing. JR Statist Soc B. 1995;57:289–300.

36. Sakakibara Y, Sekiya M, Saito T, Saido TC, Iijima KM. Cognitive and emotional alterations in App knock-in mouse models of Aβ amyloidosis. BMC Neurosci. 2018;19:46.

37. Nieraad H, de Bruin N, Arne O, Hofmann MCJ, Schmidt M, Saito T, et al. Impact of hyperhomocysteinemia and different dietary interventions on cognitive performance in a knock-in mouse model for Alzheimer's disease. Nutrients. 2020; 12:3248.

38. Hongo N, Takamura Y, Nishimaru H, Matsumoto J, Tobe K, Saito T, et al. Astaxanthin ameliorated parvalbumin-positive neuron deficits and Alzheimer's disease-related pathological progression in the hippocampus of $App^{NL-G-F/NL-G-F}$ mice. Front Pharmacol. 2020;11:307.

39. Chen Z, Zhong C. Decoding Alzheimer's disease from perturbed cerebral glucose metabolism: implications for diagnostic and therapeutic strategies. Prog Neurobiol. 2013;108:21–43.

40. Masuda A, Kobayashi Y, Kogo N, Saito T, Saido TC, Itohara S. Cognitive deficits in single App knock-in mouse models. Neurobiol Learn Mem. 2016;135:73–82.

41. Pearse DD, Hughes ZA. PDE4B as a microglia target to reduce neuroinflammation. Glia. 2016;64:1698–709.

42. Leng F, Edison P. Neuroinflammation and microglial activation in Alzheimer disease: where do we go from here? Nat Rev Neurol. 2021;17:157–72.

43. Tibbo AJ, Baillie GS. Phosphodiesterase 4B: master regulator of brain signaling. Cells. 2020;9:1254.

44. Vepsäläinen S, Hiltunen M, Helisalmi S, Wang J, van Groen T, Tanila H, et al. Increased expression of Abeta degrading enzyme IDE in the cortex of transgenic mice with Alzheimer's disease-like neuropathology. Neurosci Lett. 2008;438: 216–20.

45. Zhang Y, Wang P. Age-related increase of insulin-degrading enzyme is inversely correlated with cognitive function in APPswe/PS1dE9 mice. Med Sci Monit. 2018;24:2446–55.

46. Leal MC, Dorfman VB, Gamba AF, Frangione B, Wisniewski T, Castaño EM, et al. Plaque-associated overexpression of insulin-degrading enzyme in the cerebral cortex of aged transgenic tg2576 mice with Alzheimer pathology. J Neuropathol Exp Neurol. 2006;65:976–87.

47. Costantini LC, Barr LJ, Vogel JL, Henderson ST. Hypometabolism as a therapeutic target in Alzheimer's disease. BMC Neurosci. 2008;9:S16.

48. During EH, Osorio RS, Elahi FM, Mosconi L, de Leon MJ. The concept of FDG-PET endophenotype in Alzheimer's disease. Neurol Sci. 2011;32:559–69.

49. Mosconi L, Tsui WH, De Santi S, Li J, Rusinek H, Convit A, et al. Reduced hippocampal metabolism in MCI and AD: automated FDG-PET image analysis. Neurology. 2005;64:1860–7.

50. Minoshima S, Mosci K, Cross D, Thientunyakit T. Brain [F-18]FDG PET for clinical dementia workup: differential diagnosis of Alzheimer's disease and other types of dementing disorders. Semin Nucl Med. 2021;51:230–40.

51. Wakabayashi Y, Stenkrona P, Arakawa R, Yan X, Van Buskirk MG, Jenkins MD, et al. First-in-human evaluation of ^{18}F-PF-06445974, a PET radioligand that preferentially labels phosphodiesterase-4B. J Nucl Med. 2022;63:1919–24.

52. Zhang L, Chen L, Beck EM, Chappie TA, Coelho RV, Doran SD, et al. The discovery of a novel phosphodiesterase (PDE) 4B-preferring radioligand for positron emission tomography (PET) imaging. J Med Chem. 2017;60:8538–51.

53. Ishikawa M, Hosoi R, Kobayashi K, Nishimura T, Inoue O. Rolipram depresses [(3)H] 2-deoxyglucose uptake in mouse brain and heart in vivo. Eur J Nucl Med Mol Imaging. 2002;29:1212–5.

54. Kobayashi K, Hosoi R, Momosaki S, Koike S, Ando K, Nishimura T, et al. Enhancement of the relative uptake of 18F-FDG in mouse fibrosarcoma by rolipram. Ann Nucl Med. 2002;16:507–10.

55. Shukuri M, Terai M, Hosoi R, Nishimura T, Gee A, Inoue O. Effect of rolipram on relative 14C-deoxyglucose uptake in inflammatory lesions and skeletal muscle. Eur J Nucl Med Mol Imaging. 2005;32:163–6.

56. Rutten K, Van Donkelaar EL, Ferrington L, Blokland A, Bollen E, Steinbusch HW, et al. Phosphodiesterase inhibitors enhance object memory independent of cerebral blood flow and glucose utilization in rats. Neuropsychopharmacology. 2009;34:1914–25.

57. Giembycz MA. 4D or not 4D – the emetogenic basis of PDE4 inhibitors uncovered? Trends Pharmacol Sci. 2002;23:548.

58. Capogna M. Neurogliaform cells and other interneurons of stratum lacunosummoleculare gate entorhinal-hippocampal dialogue. J Physiol. 2011;589:1875–83.

59. Moser EI, Kropff E, Moser MB. Place cells, grid cells, and the brain's spatial representation system. Annu Rev Neurosci. 2008;31:69–89.

60. Braak H, Braak E. Entorhinal-hippocampal interaction in mnestic disorders. Hippocampus. 1993;3:239–46.

61. Negrón-Oyarzo I, Espinosa N, Aguilar-Rivera M, Fuenzalida M, Aboitiz F, Fuentealba P. Coordinated prefrontal-hippocampal activity and navigation strategy-related prefrontal firing during spatial memory formation. Proc Natl Acad Sci USA. 2018;115:7123–8.

62. Binder S, Mölle M, Lippert M, Bruder R, Aksamaz S, Ohl F, et al. Monosynaptic hippocampal-prefrontal projections contribute to spatial memory consolidation in mice. J Neurosci. 2019;39:6978–91.

63. Dodart JC, Mathis C, Bales KR, Paul SM, Ungerer A. Early regional cerebral glucose hypometabolism in transgenic mice overexpressing the V717F beta-amyloid precursor protein. Neurosci Lett. 1999;277:49–52.

64. Reiman EM, Uecker A, Gonzalez-Lima F, Minear D, Chen K, Callaway NL, et al. Tracking Alzheimer's disease in transgenic mice using fluorodeoxyglucose autoradiography. Neuroreport. 2000;11:987–91.

65. Valla J, Schneider L, Reiman EM. Age- and transgene-related changes in regional cerebral metabolism in PSAPP mice. Brain Res. 2006;1116:194–200.

66. Nicholson RM, Kusne Y, Nowak LA, LaFerla FM, Reiman EM, Valla J. Regional cerebral glucose uptake in the 3xTG model of Alzheimer's disease highlights common regional vulnerability across AD mouse models. Brain Res. 2010;1347: 179–85.

67. Locci A, Orellana H, Rodriguez G, Gottliebson M, McClarty B, Dominguez S, et al. Comparison of memory, affective behavior, and neuropathology in APP^{NLGF} knock-in mice to 5xFAD and APP/PS1 mice. Behav Brain Res. 2021;404:113192.

68. Rahimi J, Kovacs GG. Prevalence of mixed pathologies in the aging brain. Alzheimers Res Ther. 2014;6:82.

69. Gurney ME, D'Amato EC, Burgin AB. Phosphodiesterase-4 (PDE4) molecular pharmacology and Alzheimer's disease. Neurotherapeutics. 2015;12:49–56.

70. Essayan DM. Cyclic nucleotide phosphodiesterase (PDE) inhibitors and immunomodulation. Biochem Pharmacol. 1999;57:965–73.

71. Wang P, Wu P, Ohleth KM, Egan RW, Billah MM. Phosphodiesterase 4B2 is the predominant phosphodiesterase species and undergoes differential regulation of gene expression in human monocytes and neutrophils. Mol Pharmacol. 1999;56: 170–4.

72. Jin SL, Lan L, Zoudilova M, Conti M. Specific role of phosphodiesterase 4B in lipopolysaccharide-induced signaling in mouse macrophages. J Immunol. 2005;175:1523–31.

73. Naganuma K, Omura A, Maekawara N, Saitoh M, Ohkawa N, Kubota T, et al. Discovery of selective PDE4B inhibitors. Bioorg Med Chem Lett. 2009;19:3174–6.

74. Barrio-Alonso E, Lituma PJ, Notaras MJ, Albero R, Bouchekioua Y, Wayland N, et al. Circadian protein TIMELESS regulates synaptic function and memory by modulating cAMP signaling. Cell Rep. 2023;42:112375.

75. Wang L, Chen H, Tang J, Guo Z, Wang Y. Peptidylarginine deiminase and Alzheimer's disease. J Alzheimers Dis. 2022;85:473–84.

76. Mukherjee A, Song E, Kihiko-Ehmann M, Goodman JP Jr, Pyrek JS, Estus S, et al. Insulysin hydrolyzes amyloid beta peptides to products that are neither neurotoxic nor deposit on amyloid plaques. J Neurosci. 2000;20:8745–9.

77. Ren M, Guo Q, Guo L, Lenz M, Qian F, Koenen RR, et al. Polymerization of MIP-1 chemokine (CCL3 and CCL4) and clearance of MIP-1 by insulin-degrading enzyme. EMBO J. 2010;29:3952–66.

78. Ishigami A, Ohsawa T, Hiratsuka M, Taguchi H, Kobayashi S, Saito Y, et al. Abnormal accumulation of citrullinated proteins catalyzed by peptidylarginine deiminase in hippocampal extracts from patients with Alzheimer's disease. J Neurosci Res. 2005;80:120–8.

79. Delikkaya B, Moriel N, Tong M, Gallucci G, de la Monte SM. Altered expression of insulin-degrading enzyme and regulator of calcineurin in the rat intracerebral streptozotocin model and human apolipoprotein E-ε4-associated Alzheimer's disease. Alzheimers Dement. 2019;11:392–404.

80. Li H, Yang S, Wu J, Ji L, Zhu L, Cao L, et al. cAMP/PKA signaling pathway contributes to neuronal apoptosis via regulating IDE expression in a mixed model of type 2 diabetes and Alzheimer's disease. J Cell Biochem. 2018;119:1616–26.

81. Gannon M, Wang B, Stringfellow SA, Quintin S, Mendoza I, Srikantha T, et al. 14-3-3θ does not protect against behavioral or pathological deficits in Alzheimer's disease mouse models. eNeuro. 2022;9:ENEURO.0368-21.2022.
82. Kidana K, Tatebe T, Ito K, Hara N, Kakita A, Saito T, et al. Loss of kallikrein-related peptidase 7 exacerbates amyloid pathology in Alzheimer's disease model mice. EMBO Mol Med. 2018;10:e8184.
83. Uruno A, Matsumaru D, Ryoke R, Saito R, Kadoguchi S, Saigusa D, et al. Nrf2 suppresses oxidative stress and inflammation in *App* knock-in Alzheimer's disease model mice. Mol Cell Biol. 2020;40:e00467-19.
84. Myeku N, Clelland CL, Emrani S, Kukushkin NV, Yu WH, Goldberg AL, et al. Tau-driven 26S proteasome impairment and cognitive dysfunction can be prevented early in disease by activating cAMP-PKA signaling. Nat Med. 2016;22:46–53.

ACKNOWLEDGEMENTS

AUTHOR CONTRIBUTIONS

SJC and ND designed research. SJC, ND, PA, HG, PAn, and IMC acquired, analyzed, or interpreted data. SJC, ND, and PA drafted the manuscript. SJC, ND, HG, and JJ obtained funding. EP, JJ, and CT provided technical or material support. All authors reviewed and approved the final paper.

FUNDING

COMPETING INTERESTS

The authors declare no competing interests.

ADDITIONAL INFORMATION

Supplementary information The online version contains supplementary material available at https://doi.org/10.1038/s41386-024-01852-z.

Correspondence and requests for materials should be addressed to Steven J. Clapcote.

Reprints and permission information is available at http://www.nature.com/reprints

Publisher's note Springer Nature remains neutral with regard to jurisdictional claims in published maps and institutional affiliations.